Title

Quantifying the impact of woody material on leaf area index estimation from hemispherical photography using 3D canopy simulations

Authors

William Woodgate[a,b,c]*, John D. Armston[d,e], Mathias Disney[f,g], Simon D. Jones[a,b], Lola Suarez[a,b], Michael J. Hill[h], Phil Wilkes[a,b,f,i], Mariela Soto-Berelov[a,b]

Author affiliations

[a] *School of Mathematical and Geospatial Sciences, RMIT University, GPO Box 2476V Melbourne, VIC, 3001, Australia*

[b] *Cooperative Research Centre for Spatial Information, Carlton, VIC 3053, Australia*

[c] *Oceans and Atmosphere, Commonwealth Scientific and Industrial Research Organisation, Yarralumla, ACT, Australia*

[d] *Remote Sensing Centre, Science Delivery, Queensland Department of Science, Information Technology, and Innovation, 41 Boggo Road, QLD 4102, Australia*

[e] *Joint Remote Sensing Research Program, School of Geography, Planning and Environmental Management, University of Queensland, St Lucia, QLD 4072, Australia*

[f] *Department of Geography, University College London, Gower Street, London, WC1E 6BT, UK*

[g] *NERC National Centre for Earth Observation, UK*

[h] *Department of Earth System Science and Policy, University of North Dakota, Clifford Hall, 9011, 4149 University Drive, Grand Forks, ND, 58202, USA*

[i] *ITC, University of Twente, PO Box 217, NL-7000 AE Enschede, the Netherlands*

* Corresponding author at: Room 27, Level 11, Building 12, Remote Sensing Centre, School for Mathematical and Geospatial Sciences, RMIT University, Melbourne, Australia

Phone: (+61) 3 9925 2472

Email: william.woodgate@rmit.edu.au

Key words

Leaf Area Index, Clumping, Alpha, Projection function, Woody correction, Plant Area Index

Highlights

1. An indirect method to estimate the woody surface area proportion in forests was validated
2. A 3D modelling and simulation framework was implemented for highly detailed 3D models
3. Sensitivity to stem distribution, stem density and PAI values was quantified
4. The method agreed to within 0.05 α of reference values and was robust to canopy structure variations

Abstract

Estimating the proportion of woody-to-total plant material 'α' is an essential step to convert Plant Area Index 'PAI' estimates into Leaf Area Index 'LAI'. α has also been shown to have a significant impact on the passive optical remote sensing signal for retrieval of biophysical parameters in forests, woodlands, and savannas. However, benchmarked indirect α retrieval methods are lacking and thus it is common for this pivotal correction to be ignored. In this paper we validate an α retrieval method using a 3D radiative transfer simulation framework, enabling the retrieval method to be benchmarked against a known and precise model truth. The 3D framework consists of a representative and highly detailed 3D explicit Eucalypt forest reconstructed from field measurements. The 3D structure is coupled with a 3D scattering model to enable simulation of remote sensing instruments. The retrieval method utilises classified hemispherical photography 'HP', but is applicable to all ground-based optical instruments that can separate leaf and woody elements. The method is applicable to evergreen forests and thus independent of the estimation of PAI or LAI. The unknown degree of mutual shading or occlusion of leaf and woody elements was traditionally a key impediment to the operational use of this method and was therefore closely examined. The indirect α method utilising classified HP imagery agreed on average to within 0.01 α of the reference (α_{ref} = 0.37). In addition, the method demonstrated robustness to a range of LAI, stem density, and stem distribution values, matching to within ±0.05 α of the reference. Angular dependence on indirect α retrieval was also found; where the entire HP image (180° FOV) was needed to produce the most accurate estimate. Conversely, the classified narrow view zenith angle range around 55-60° zenith also provided an α estimate matching the reference. At this narrow zenith angle the method is insensitive to leaf angle distribution. As such, careful consideration of zenith angle range utilised from the instrument is recommended. The results demonstrate the method's applicability for accurate indirect estimation of α in single-storey forest types.

The simple and efficient method can be used to convert estimates of PAI into LAI from a variety of optical ground-based instruments. Quantitative α estimates can and should be used to aid interpretation of the remote sensing signal from satellite imagery, which has been shown to be sensitive to the proportion and spatial distribution of woody canopy materials.

Introduction

Leaf Area Index (LAI) is a primary descriptor of vegetation function and structure, and an essential climate variable (GCOS, 2011). It is usually defined as the total one-sided area of leaf tissue per unit of ground area (Chen & Black, 1992). *In situ* LAI estimates are extensively used to validate LAI products from remote sensing data among other purposes (Camacho et al., 2013; Garrigues et al., 2008). Earth-observation derived LAI estimates are used more widely in Earth System Models as the main interface for water, energy and mass exchange, e.g. (Kowalczyk et al., 2013).

Estimation of the woody-to-total plant area proportion (α) enables disaggregation of Plant Area Index (PAI) into LAI and Woody Area Index (WAI) (Chen, 1996). Many studies do not attempt to apply the α correction factor to PAI estimates, e.g. Hardwick et al. (2015); Tang et al. (2014). This is problematic for accurate LAI estimation due to typical values of α in forests ranging from 0.1 to 0.4 (Gower et al., 1999). Uncorrected LAI estimates therefore risk overestimation. α also has a secondary significance for indirect LAI estimation methods based on application of the *Pgap* model, used for the estimation of the combined projection function *G* of leaf and woody components (Woodgate et al., 2015a). The accurate retrieval of α is then a critical step in the estimation of LAI from ubiquitous indirect LAI estimation methods (see extensive reviews by (Bréda, 2003; Jonckheere et al., 2004; Zheng & Moskal, 2009)). Additionally, in order to be part of global biophysical parameter estimation the α retrieval method needs to be applicable across different forest types.

Direct methods based on destructive estimates of woody area have traditionally been regarded as the most accurate due to the potential to completely quantify leaf and wood material independently. Examples of studies relying on direct methods include Deblonde et al. (1994) and Gower et al. (1997). Such manually intensive methods are dependent on species composition and growth form and rarely carried out at anything other than small scales and for low stature vegetation (Hagihara & Yamaji, 1993).

Indirect estimates of α have the advantage of being comparatively efficient and non-destructive. A number of indirect methods have been employed which mainly vary in instrumentation used and applicability to deciduous or evergreen species. A commonly employed method in deciduous forests is to estimate PAI in leaf-on conditions, and then repeat the measurements in leaf-off conditions to estimate the Woody Area Index 'WAI'; where α = WAI:PAI (Chen et al., 1997a; Leblanc & Chen, 2001). Leblanc & Fournier (2014) in a 3D modelling framework found two processing techniques that on average provided estimates of WAI within 10% of the model truth (see their Table 6), due to errors cancelling out from estimating PAI in leaf-on conditions and WAI in leaf-off conditions. An alternative to this method is to estimate PAI, and then mask out woody material for applicable methods to estimate an approximation of LAI (Liu et al., 2012). However, the application of a masking technique requires careful consideration of the underlying assumptions (and limitations) regarding the spatial distribution of wood and foliage. This is discussed further below. New developments with accurate 3D reconstruction of trees gives rise to another potential α estimation method, e.g. (Calders et al., 2015; Côté et al., 2009; Raumonen et al., 2013). Total woody area and thus WAI can be calculated through querying total (known) woody area of reconstructed trees. A challenge of this method is to have reconstructed 3D models with accurately separated leaf and high order branch area, which is required to accurately determine α.

Sea et al. (2011) estimated α as a simple proportion of woody cover to total tree cover from classified hemispherical photography (HP) images. α was determined as the slope of the linear fit between wood cover fraction and total tree cover fraction for all classified images. This method assumes that woody material and leaf material are distributed approximately evenly throughout the canopy. In other words, the assumption is made that the visible cover proportion is equivalent to true surface area proportion, as α is an area-based metric. The classified material proportions from the images were stable in a savanna environment spanning a 900 km transect in Northern Australia, indicating the applicability of a single α correction factor across an ecological gradient. Sea's method is applicable to evergreen forests and is independent of estimation of PAI and LAI. The method is also applicable to other instruments capable of classifying woody and leaf material, e.g. single or dual-wavelength Terrestrial Laser Scanners (TLS) (Danson et al., 2014; Malenovský et al., 2008), digital cover photography (Macfarlane et al., 2007b), and the multiband vegetation imager (MVI) instrument developed to separate non-photosynthetic from photosynthetic material and sunlit from shaded material (Kucharik et al., 1997).

The spatial distribution of wood with respect to leaf material, such as mutual shading or occlusion, needs to be carefully considered for indirect methods utilising classification or image masking procedures. The importance of mutual occlusion is potentially enhanced if instruments or methods are only operating at a narrow or small view zenith angles where stems are not visible, yet are known to contribute significantly to PAI. Such issues to date have not been comprehensively explored. These issues highlight the reasons why indirect techniques would benefit from benchmarking against precisely known or 'true' values to evaluate method accuracy and better elucidate potential limitations.

Traditionally a single α value is provided for a forest plot or region. However, when measured via indirect optical methods, it is possible to characterise the degree of mutual shading or occlusion of wood and leaf components as a function of view zenith angle. Characterising how this view-angle specific or 'effective' α estimate from indirect optical methods relates to the true α is essential for better understanding photosynthetic processes and its impact on carbon sequestration and net primary production (Whittaker & Woodwell, 1969). In addition, the proportion and spatial distribution of the woody material in a canopy has a significant impact on the bidirectional reflectance factor (BRF) measured from remote sensing platforms (Asner, 1998; Malenovský et al., 2008), being critical for pigment foliar retrievals at the canopy scale (Verrelst et al., 2010). Few studies have explored the relationship between effective α estimates from indirect optical methods to the true α value, mainly due to difficulties in retrieving a highly accurate α estimate. There are still knowledge gaps around which zenith angle range to use from optical methods that can distinguish foliage from wood, and the method's robustness to varying LAI values, stem configurations and canopy structures.

Evaluation of indirect retrieval methods may be compromised by potential errors in the *in situ* validation or benchmarking methods, which themselves are also subject to large errors (Chen et al., 1997b). Furthermore, validation of these indirect methods in forested environments are lacking in the literature, for the reasons outlined above. Only a small number of studies, representing a handful of forest types (real or virtual), have benchmarked α optical retrieval methods, e.g. Leblanc & Fournier (2014); Kucharik et al. (1998). There is a need to quantify α retrieval method accuracies so that they may be implemented with confidence. Further assessment of retrieval method strengths and limitations in representative forested environments is required.

An attractive alternative to benchmarking field-derived LAI and α estimates is through 3D computer simulation model frameworks, e.g. Leblanc & Fournier, (2014); Walter et al. (2003). This approach enables simulation of indirect retrieval methods, which can then be tested against modelled 3D canopy structure, where the wood and leaf area (and angular distribution) are known precisely *a priori*. Other advantages of a detailed 3D modelling approach are the flexibility in using a wide range of synthetic or 'virtual' 3D scenes. A potential trade-off is the considerable complexity, resources, time, and high degree of skill required to create a representative 3D virtual forest environment. Computing resources are typically no longer a limitation.

A select few studies have implemented 3D modelling frameworks to validate indirect LAI or PAI retrieval methods. Of those that have, ray tracing models coupled with a limited degree of canopy architectural realism were employed, e.g. (Disney et al., 2011; Jonckheere et al., 2006; Leblanc & Fournier, 2014). Of these 3D modelling studies, only Leblanc & Fournier (2014) evaluated the accuracy of a method to indirectly estimate α utilising HP. However, a key limitation of the method tested was the requirement of leaf-on and leaf-off canopy conditions, thus limiting its application to deciduous forests. In addition, mutual shading of leaf and woody components and the effect of instrument view zenith angle were not explored.

The primary objective of this study was to use a 3D modelling approach to validate the α retrieval method implemented by Sea et al. (2011) utilising classified HP. Secondary objectives of this study included establishing the sensitivity of the indirect optical method to increasing LAI values, different stem distributions and different viewing angle configurations. The simulation framework was applied to a 3D forest canopy of a high degree of architectural realism reconstructed from empirical data, representative of a Box Ironbark Eucalypt forest in eastern Australia (Woodgate et al., 2015a). We specifically focused on the 55-60° view zenith angle range due to the known convergence of leaf and wood angle distributions near the 57.3° angle (Nilson, 1971; Wilson, 1963; Woodgate et al., 2015a). We conclude by discussing the implications of our results and identify priority areas for future research.

Materials and Methods

Study site and data collection

The Rushworth Box Ironbark forest study site (36°45’S, 144°58’E) was selected following the 3D reconstruction methodology in Woodgate et al. (2015a). Rushworth is representative of a dry sclerophyll forest comprised of several Eucalyptus (*E*) tree species. The trees are typically 10-15 m tall with an average stem density of 520 stems ha^{-1}. The single strata site is also characterised by low-lying undulating land and a lack of understorey presence. The 3D trees were reconstructed from field measured forest plot inventory data to reflect key structural attributes of *E* species such as their moderate degree of within-crown clumping and predominant erectophile leaf angle distribution (Jacobs, 1955).

High-resolution hemispherical photography (HP) was captured at eight plot locations in the Rushworth. In each plot, 13 HPs were captured using the sampling scheme derived from the Statewide Landcover and Trees Study (SLATS) transects, developed to estimate foliage projective cover (among other metrics) for calibration and validation of remotely sensed products (Armston et al., 2009; Schaefer et al., 2015). HPs were spaced 25 m apart on three intersecting 100 m transects, oriented at 60 degrees from one another (**Figure 1**). The HP processing protocol was that of the two-corner (TC) classification method, using the dual binary threshold, which produced binary classified images of sky and non-sky (Macfarlane, 2011; Woodgate et al., 2015b). Airborne LiDAR Scanning (ALS) data were concurrently acquired over the Rushworth forest inventory plots. ALS was flown with a RIEGL LMS-Q560 laser scanner (Horn, Austria) covering a 25 km^2 area with a flying height < 600 m, mean footprint diameter of 30 cm, and a pulse density of 6-10 pulses m^{-2} (Wilkes et al., 2015). Post-processing was conducted in RIEGL RiAnalyze® (version 4.1.2), resulting in a discrete return dataset of up to 6 returns (absolute accuracy: ±20 cm horizontal, ±30 cm vertical). The ALS and HP image datasets were used to validate the virtual scenes (**section 2.3**).

LAI retrieval based on the gap fraction model (*Pgap* model)

LAI is typically estimated from optical instruments by solving for LAI through the Beer-Lambert law as described in Nilson (1971). The physical formulation has subsequently been modified to incorporate a correction for the proportion and the angular contribution of woody components by Chen (1996) and by Woodgate et al. (2015a), respectively. This formulation is also referred to as the *Pgap* model, solved for LAI from independent structural parameters:

$$LAI = \frac{-\log Pgap_T(\theta)\cos(\theta)(1-\alpha)}{G_T(\theta)\Omega_T(\theta)} \quad \textbf{[1]}$$

Where $Pgap_T(\theta)$ is the gap probability of all canopy elements (leaf and wood) as a function of view zenith angle (θ), $G_T(\theta)$ is the combined projection coefficient of wood $G_W(\theta)$ and leaf $G_L(\theta)$ elements characterising the angular contribution of both leaf and woody facets (Ross, 1981; Woodgate et al., 2015a), $\Omega_T(\theta)$ is the combined clumping factor of all canopy elements relating effective LAI (LAIe) to true LAI via LAI = LAIe(θ) / $\Omega_T(\theta)$, and α is the ratio of woody-to-total plant area, also referred to as the woody element correction factor. Here α is independent of the spatial distribution of woody material, i.e. it only corrects for the proportion of woody material. **Eqn. 1** assumes all canopy elements are non-preferentially oriented in azimuth.

G_T in **Eqn. 1** relates to woody G_W and leaf G_L projection function coefficients through α as a weighting parameter (Woodgate et al., 2015a):

$$G_T(\theta) = (1-\alpha)G_L(\theta) + \alpha.G_W(\theta) \quad \textbf{[2]}$$

3D modelling of forest scenes

Virtual 3D representations of the forest environment or 'scenes' were simulated using *librat* (Lewis, 1999), a 3D Monte Carlo ray tracing model used for benchmarking other radiative transfer models in the Radiation Model Intercomparison (RAMI) exercise (Widlowski et al., 2013). Here, a total of 24 scenes were simulated comprising different PAI values and stem distributions as described in **Table 1**. The 24 scenes are a product of multiplying the six stem distributions with four PAI values. The scene α values (α_{0m} = 0.38, $\alpha_{1.5m}$ = 0.36) are at the upper end of the typical range of forests reported in the literature (Gower et al., 1999; Kucharik et al., 1998).

Table 1. Virtual Scene parameters for the 24 simulated scenes.

Stand Values	
Domain X, Y	270 m, 270 m
Stem distribution (*v:m*)	Regular (0.5), Random (1), Neyman (1.5, 2, 3, 5)
Number of species	5
Leaf Angle Distribution*	Erectophile
Stem density (*trees* ha^{-1})	230, 460, 690**
LAI (PAI)^	0.38 (0.61), 0.76 (1.21), 1.14 (1.82), 1.5 (2.41)
WAI:PAI 'α'	0.36

(*v:m*) refers to the variance to mean ratio of a stem distribution (Franklin et al., 1985). *denotes the erectophile LAD from De Wit (1965). **denotes the 689 stem density was used for scenes with PAI = 1.8 and 2.4. ^ denotes values for > 0 m above ground; scene PAI values above 1.5 m (camera height) are $0.97\mathrm{x}PAI_{0m}$ for all scenes, α > 0 m is 0.38 for all scenes, scene LAI values > 1.5 m are unchanged.

Six stem distributions were implemented to simulate different degrees of between-crown clumping. One regular, one random, and four clumped stem distributions of varying degree were implemented for each scene LAI value. The degree of stem clumping was quantified through the variance-to-mean ratio (*v:m*) of the number of stems per quadrat for a given quadrat size in an x, y domain (Franklin & Spies, 1991). A quadrat size of 15 m x 15 m was chosen to replicate the stem distributions, which coincided with the approximate extent of radiation interaction between trees, i.e. the horizontally-projected path length of a solar beam through the canopy, as recommended by Chen & Leblanc (1997). The *v:m* intervals chosen for each simulated stem distribution encompassed the range in the measured field inventory plots at the 15 m quadrat size and also deliberately exceeded them in order to test the sensitivity of retrieval methods to more extreme stem clumping values (measured range: 0.6 – 1.3 *v:m*, **Figure A1**; simulated range: 0.5 – 3.5 *v:m*, **Table 1**). The original scene domain of the quadrats was 90 m x 90 m, providing 36 quadrats. The original domain was then cloned 8 times to produce a 270 m x 270 m scene domain in a 3 x 3 grid configuration; avoiding edge effects when sampling with simulated HPs. Additional information on the stem placement and virtual scene configuration can be found in **Appendix A** to aid manuscript clarity.

Simulation of hemispherical photographs (HPs) and canopy cover maps

HPs were simulated in 'reference' mode to simulate true gap fraction determined from ray intersection. For every pixel in the image FOV, a single ray is traced from the camera position in the direction of the pixel centroid to determine if there is a canopy intersection event returning a binary result; '0' for a canopy intercept or '1' for a gap. This method effectively produces pre-classified 'reference' HP images, thus avoiding potential *Pgap* classification errors that would otherwise confound interpretation of results. The material type for every intercepted pixel was also recorded in a separate image, i.e. wood or leaf intercept, hereafter referred to as the classified HP image, without error. This approach is far more computationally efficient than stochastic ray tracing of the full light environment (Jonckheere et al., 2006), which can require three wavelengths and multiple sampling rays per pixel to provide an RGB image (Disney et al., 2000).

Virtual scene cover maps (90 m x 90 m; **Figure 1**) were simulated in *librat* at 1 cm resolution, based on a solitary ray traced at the centroid of each pixel returning the first intercept height from above the canopy; used to derive canopy height profiles.

Figure 1: SLATS sampling design

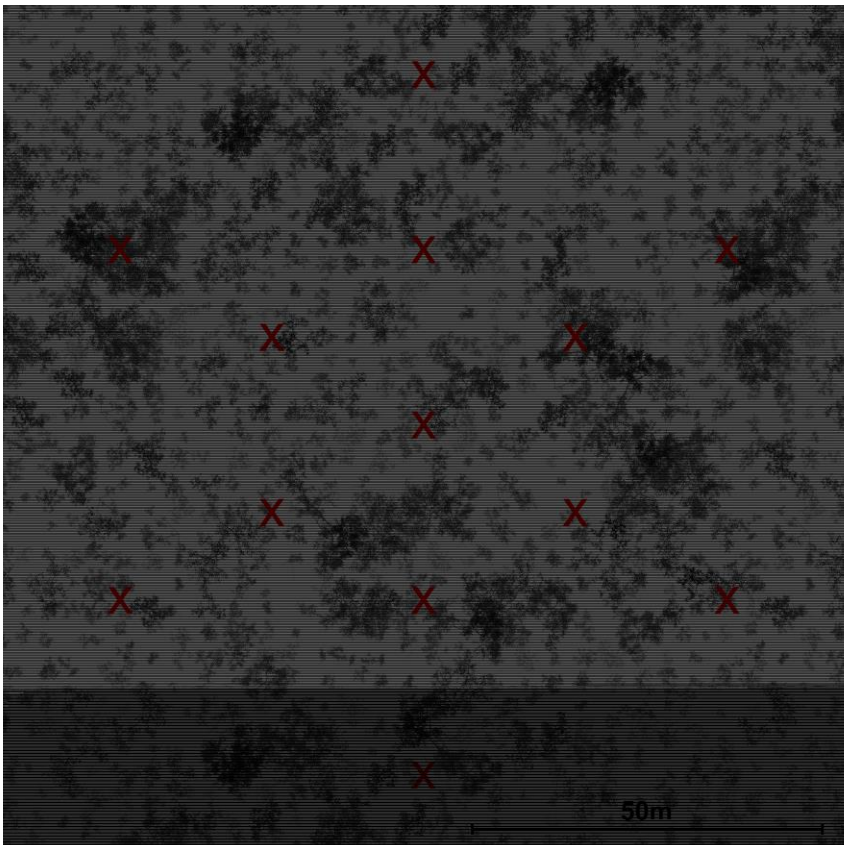

Figure 1. Sample locations of the 13 HPs from the SLATS transect design (red crosses) overlayed on a 120 m x 120 m element cover map simulation of the regular stem distribution (1.8 PAI).

In each virtual scene, 13 HPs were simulated using the SLATS sampling scheme previously described (**Figure 1**). In this study, 13 HPs were deemed an appropriate number per scene as: (i) it met the minimum recommended plot sample number (≈8-10 HPs) of various protocols (Baret et al., 2005; Fernandes et al., 2014; Homolová et al., 2007), in addition to (ii) representatively sampling an approximate 100 m x 100 m plot at the centre of the scene domain.

The centre of the sampling design was coincident with the centre of the 270 m x 270 m scene domain. HPs were simulated at 1.5 m above ground level, pointing directly upwards with 180°

hemispherical field-of-view (FOV). A minimum separation distance of 30 cm between measurement and tree stem location was ensured. The HP image resolution was set to 3001 x 3001 pixels, which is equivalent to a 12 megapixel digital camera with a 4:3 image format.

Although sampling design can play an important role in the retrieval methods (e.g. spatial representativeness), it was not a focus of this investigation. The variability of the scene *Pgap* as sampled by HPs is provided in **section 3.1** of the Results and Discussion. A brief discussion on the implications of sampling position is provided later in the manuscript.

Comparisons of simulated model outputs with HP and ALS field measured data were made. The purpose was twofold: the first comparison was to inform which simulated scenes' *Pgap* provided the closest match with *Pgap* derived from HP captured at Rushworth; the second was to provide additional evidence that the canopy density distributions via the height profiles of the modelled scenes were reflecting the Rushworth forest as measured from comparable independently collected ALS data. Normalised first return ALS profiles of the classified canopy returns from 100 m x 100 m plots coincident with the HP sample locations were compared with canopy height profiles simulated from the virtual scenes.

Reference woody-to-total plant area calculation

The reference α value for each virtual scene was calculated directly from the tree models leaf and wood area:

$$\alpha_{ref} = \frac{\sum(wood\ area)}{\sum(wood\ area)+\sum(leaf\ area)} = \frac{WAI}{WAI+LAI} = \frac{WAI}{PAI} \quad \textbf{[3]}$$

As **Eqn. 3** provides an exact quantification of α or reference value, it is hereafter referred to as α_{ref}. In contrast to any *in situ* retrieval method, which only ever approximate the 'true' value, α_{ref} from the 3D model is the true value, and can thus be used to benchmark any retrieval method values.

Woody-to-total area ratio estimation following Sea et al. (2013)

The previously mentioned indirect α retrieval method from Sea et al. (2011) formed the basis of the evaluation. Here, the simulated reference classified HPs outlined in **section 2.3** were utilised, ensuring image classification error would not confound results. Using this method, α was estimated, hereafter referred to as α_{est}, as the proportion of woody cover to total plant cover, i.e. α_{est} = ∑woody pixels / (∑woody pixels + ∑leaf pixels). The method is applicable to other instruments capable of classifying woody and leaf material, e.g. single or dual-wavelength Terrestrial Laser Scanners (TLS) (Danson et al., 2014; Malenovský et al., 2008) and digital cover photography (Macfarlane et al., 2007b). The method is also applicable to evergreen forests and is independent of PAI and LAI estimation.

The accuracy of the method was determined by direct comparison of α_{est} with the scene α_{ref} values, calculated from the known wood and leaf area of the constituent tree models (**section 2.4**). The impact of restricting the HP FOV was then analysed to determine whether the entire FOV was required to obtain an accurate estimate. The sensitivity of the method to the simulated scene PAI values and stem distributions was then established through grouping α_{est} and significance testing, further explained in **Section 2.6**.

Statistical analysis

Two-way analysis of variance (ANOVA) was conducted to detect significant differences between factors such as scene PAI and stem distribution for α values. If the ANOVA revealed significant differences ($p < 0.05$), Tukey's honest significance difference (HSD) test was conducted post-hoc to determine which combination of factors had significant differences. Statistical analysis was conducted in IBM SPSS Statistics v22 (IBM Corp).

Results and Discussion

Architectural model performance

This section presents a comparison of simulated virtual scene outputs with independently collected field data to establish the degree of matching of the 3D reconstructed environment with the real Box Ironbark Eucalypt forest. Specifically, the key structural metrics of gap probability (*Pgap*) and canopy height profiles are compared. Woodgate et al. (2015a) previously demonstrated the close degree of matching of individual tree reconstructions with empirical data.

A visual comparison of a simulated HP in reference mode with a classified field measured HP from Rushworth is shown in **Figure 2**. The average scene *Pgap* for each of the four simulated PAI values (n = 78 HPs per PAI value) was calculated and compared against the mean *Pgap* for all the field measured HPs at Rushworth (n = 104) (**Figure 3**). The mean of the field measured HP *Pgap* from RF plots matched within ±0.05 *Pgap* with the mean simulated HP *Pgap* for the PAI = 1.8 scenes. The field-derived *Pgap* was also well within the range of the virtual scene *Pgap* from all virtual scenes. The field-derived HP *Pgap* typically matched to within ±0.05 *Pgap* of the mean of PAI = 1.8 scene simulations, showing a similar variance and extinction curve over all zenith angles.

Figure 2: Simulated and field-derived Hemispherical Photos

(a) (b)

Figure 2. Comparison of a simulated HP images in reference mode (a), with a classified field measured HP image (b) at Rushworth. The simulated image was taken from the Neyman scene (*v:m* = 2, LAI = 1.5), and the field measured HP was from a field plot with estimated LAI = 1.2; estimated from site-specific allometric plot data described in Woodgate et al. (2015a).

Pgap from the 90 m x 90 m cover maps is also presented in **Fig. 3**. The mean simulated HP *Pgap* matched to within ±0.02 *Pgap* of the cover maps for PAI scene values = 0.6, 1.2, and 1.8. However, there was a 0.05 *Pgap* difference for the PAI = 2.4 scenes. Although the two methods are sampling the same virtual scenes, discrepancies are likely caused by the nature of incomplete HP sampling, well documented in previous studies, e.g. (Macfarlane et al., 2007a). Additionally, differences between ALS *Pgap* and field-derived HP *Pgap* at the 5° view zenith angle (VZA) are within expected uncertainty tolerances due to well-known issues of sampling and processing to name a few, e.g. (Armston et al., 2013; Lovell et al., 2003).

Figure 3: *Pgap* of simulated and field-measured data

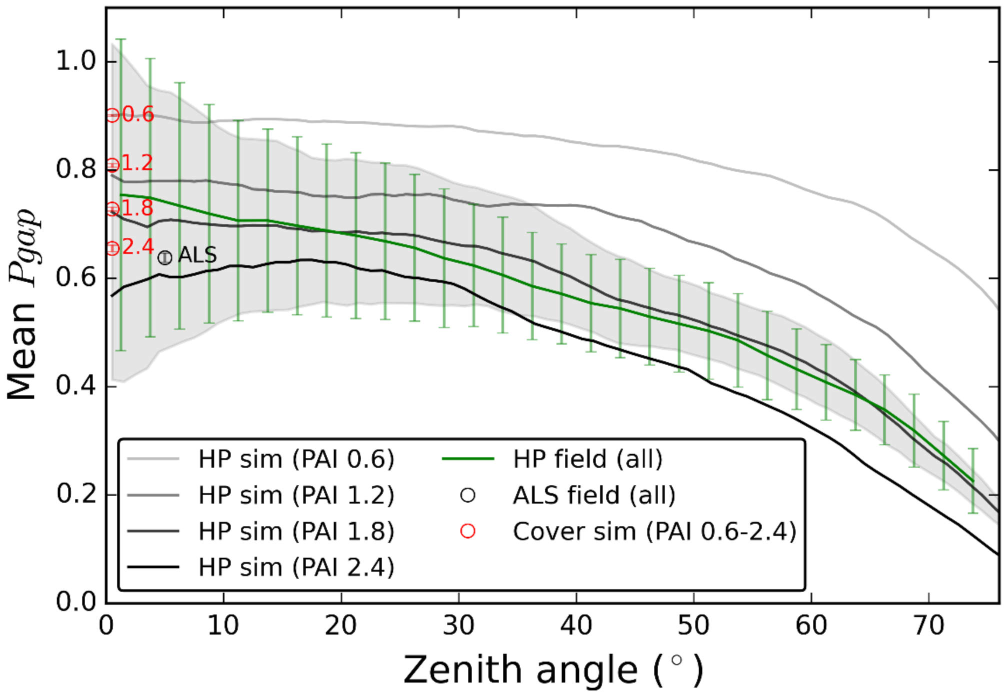

Figure 3. *Pgap* of simulated reference height maps and simulated HPs overlayed with field measured HPs and ALS *Pgap*. The solid grey-scale lines denote the azimuthally averaged simulated 'sim' HP mean *Pgap* of each individual PAI scene value (PAI = 0.6, 1.2, 1.8, 2.4; n = 78 HPs per PAI value), with ± 1 standard deviation (SD) shaded in grey around the PAI = 1.2 scene simulations; the green line denotes the azimuthally averaged field measured HP mean *Pgap* with ± 1 SD error bars of all the field measured HPs at Rushworth at plots RF1-7 and 9 (RF8 not measured; n = 104 HPs); red circles at zenith = 0° denote the mean and SD *Pgap* from the simulated 90 m x 90 m element cover maps for the four PAI scene values, annotated with their PAI value (red text), treated as reference due to their complete coverage and 1 cm x 1 cm resolution; and the black circle at the 5° zenith angle denotes the mean and SD *Pgap* of the nine coincident 100 m x 100 m ALS plots to the field measured HPs, using the weighted return method (Lovell et al., 2003) - marker placed at 5° zenith due to ± 10° ALS look angle, annotated with 'ALS' in the figure.

Overall the normalised height profiles of the field measured ALS showed good agreement with the simulated profiles of all four simulated PAI scene values. This indicated the distribution of simulated canopy materials in the height domain was accurately represented (**Figure 4a**). For example, the location of the tails of the simulated and ALS profiles closely align; representing the lower and upper bounds of the single-storey canopy at Rushworth. The first three simulated PAI value scenes (PAI = 0.6, 1.2, 1.8) have a slightly closer agreement to the ALS profiles than fourth PAI value scenes (PAI = 2.4). Further discussion on the height profiles from the virtual scenes and ALS data can be found in **Appendix A**.

Figure 4: Height profiles and reference element area

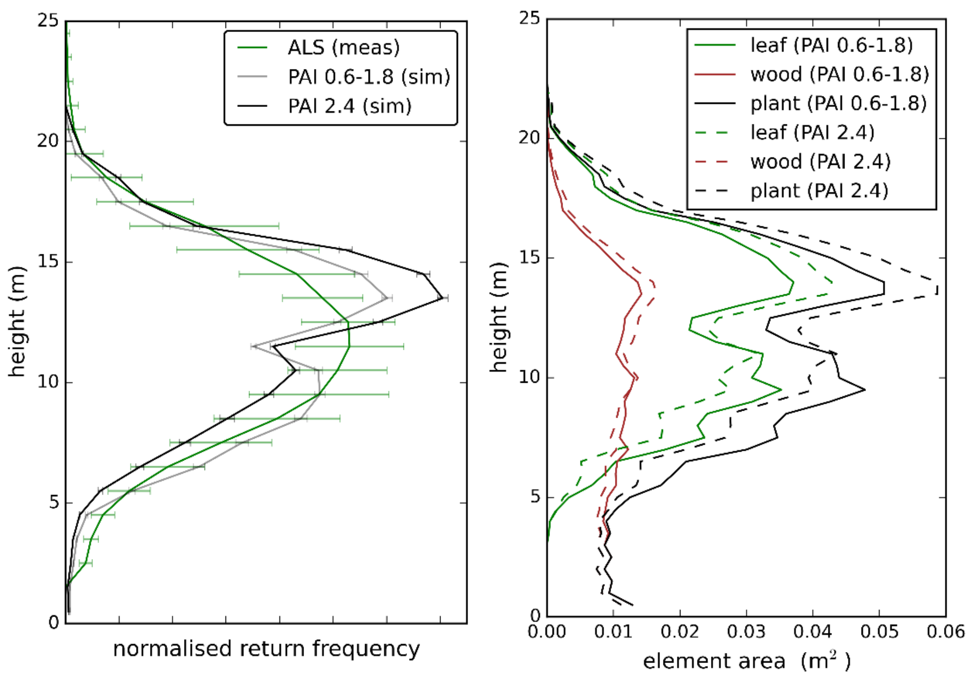

(a) (b)

Figure 4. (a) Height profile comparison of measured ‘meas’ ALS flown at Rushworth using the mean of all nine 100 m x 100 m plots centered on the plot locations (green line) and ± 1 standard deviation (SD; green error bars), with height profiles from the simulated ‘sim’ plots using *librat*. Simulated scenes were grouped into PAI values 0.6, 1.2, and 1.8 (grey line) and PAI

= 2.4 (black) with ± 1 SD error bars. The bin size is 1m. All returns are non-ground 1st return. **(b)** Element area for the simulated scenes of leaves (green lines), wood (brown lines), and plant (leaf and wood together; black lines). Element area was calculated from the summation of the 3D tree model facet area comprising a scene. The first three PAI value scene groupings (PAI 0.6, 1.2, 1.8) have the same element area frequency (solid lines), and the PAI = 2.4 scenes have a different frequency (dashed lines). The bin size is 0.5m.

Retrieval of woody-to-total plant area

The method of Sea et al. (2011) to indirectly determine the woody-to-total plant area correction factor 'α_{est}' was validated using the 3D modelling and simulation framework. **Figure 5** shows tree cover fraction plotted against wood cover fraction from simulated classified HP for all images in every scene (n = 312). Tree cover from 0.1 to 0.7 was found for all simulated HPs, which is equivalent to canopy closure '*cc*' (Jennings et al., 1999). Sea et al. (2013) utilised the gradient of the fitted linear reduced major axis (RMA) regression function as a proxy for α_{ref}. The gradient of the slope in **Figure 5** was 0.37, with a coefficient of determination R^2 = 0.89. The slope matched to within 0.01 of α_{ref} above the camera height (α_{ref} = 0.36) for the Rushworth virtual scenes. The match demonstrated the utility of this method for accurate indirect estimation of α from classified HPs in the Box Ironbark forest type.

Figure 5: Tree cover vs wood cover fraction

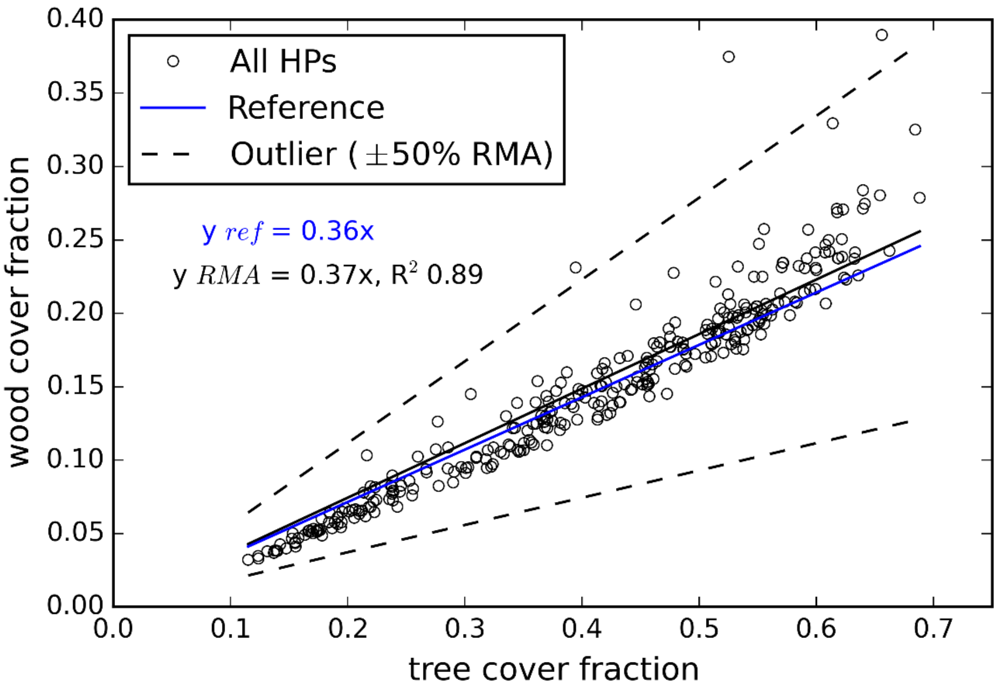

Figure 5. Total tree cover fraction plotted against the total wood fraction for all 312 simulated classified HPs denoted by open black circles. Tree and wood cover fractions were calculated as

the proportion of leaf and wood pixels, and wood-only pixels, to total HP image pixels, respectively. The entire field-of-view 'FOV' (i.e. 0-90° view zenith angle) of the classified HPs were used. The α_{ref} slope 'y *ref*' is denoted by the solid blue line. The RMA regression slope 'y *RMA*' is denoted by the solid black line, with error bounds of ± 50% to identify potential outliers in dashed black lines.

Three outliers from of a total 312 HPs were detected, determined as ±50% from both the reference and RMA regression slopes (**Figure 5**). All outliers overestimated α_{ref}. Upon further examination, the outliers were HPs with very large stems in close proximity to the HP measurement location (<1 m; e.g. **Figure 6**), which led to a greatly increased visible proportion of wood-to-total plant material. Therefore, a recommendation would be to ensure a minimum distance of ≈1.5 m from the base of any proportionately large stems to HP measurement location to negate the bias. Stands with a relatively large proportion of senescent trees could also result in similar outliers. This introduces a potential limitation of the representativeness or applicability of a single α value characterising an entire forest type.

Figure 6: Outlier HPs with a high wood-to-total plant area ratio

1. α_{ref} = 0.58 2. α_{ref} = 0.71 3. α_{ref} = 0.59

Figure 6. The three α_{est} outlier HP images identified in **Figure 5**. The individual HP image α_{ref} value (shown) was estimated as the proportion of woody pixels to total plant pixels from the

simulated classified HPs. All images were located close to large tree stems, which positively biased the proportion of wood-to-total plant material visible in the image. The respective PAI scene values and stem distributions of the three HPs are: **(a)** PAI = 0.6 (Neyman *v:m* 5), **(b)** PAI = 1.2 (Random), and **(c)** PAI = 2.4 (Random).

Conversely, no outliers less than 50% of α_{ref} were found. This was due to the combination of foliage bearing branches starting approximately 5 m above the ground as shown in **Figure 4b**, and HPs sampled near ground level (1.5 m). Potential outliers underestimating α_{ref} would be expected in environments where understorey near to the camera is prominent, thus the recommendation to take HPs both above and below understorey has been made in numerous protocols e.g. (Leblanc, 2008; Schaefer et al., 2015). It is also important to consider whether understorey is included in the α metric, which would potentially bias HP sampling due its close proximity to the camera lens.

The effect of restricting field-of-view (FOV)

The entire HP FOV (typically 180° for fisheye lenses) is rarely utilised in analysis, due to multiple factors affecting the accurate classification of pixels for large zenith angles, including undulating terrain and a greater proportion of mixed pixels (Jonckheere et al., 2004; Leblanc et al., 2005). Therefore, it is common practise to either restrict the instrument FOV to a maximum zenith angle for indirect LAI estimation and subsequent estimation of α_{est} (e.g. Sea et al., 2011), or to use a discrete narrow zenith angle range (e.g. Neumann et al., 1989; Leblanc & Fournier, 2014).

The effect of restricting instrument FOV was investigated. The slope of the RMA line of tree cover fraction versus woody cover fraction when restricting the HP FOV to 140° (i.e. 0-70° zenith angle range) decreased from 0.37 to 0.34 (R^2 = 0.87). This indicated a slightly poorer agreement with α_{ref} = 0.36 (RMA graph not shown). The dependence of α_{est} derived from classified HPs on view zenith angle is shown in **Figure 7**. The mean α_{est} of all 312 simulated HPs (red line; **Figure 7**), a proxy of the RMA slope, increased with zenith angle from 0.15 at 0° to close to 1 at 90°. This indicates as expected that the assumption of a random or even distribution of woody material with respect to leaf material as a function of viewing angle does not hold. There was also a large spike in mean α_{est} values at zenith angles greater than 75°, likely caused by the fact that at very large zenith angles predominantly stems are visible, due to a moderate 3.5 m gap between crown break and the height of the HP measurements as shown in **Figure 4b**.

Interestingly, the mean α_{est} at around 56° zenith angle matched with α_{ref}, meaning that the visible proportion of woody-to-total plant material at this narrow zenith angle range was equivalent to the reference value. This narrow zenith angle range offers an alternative to utilising the entire image FOV to accurately estimate α_{est}, at least for the forest type investigated. The slope of the mean α_{est} line in **Figure 7** would be expected to change with different leaf angle distributions (LAD). The exception to this would be at the 57.3° viewing angle where the mean α_{est} would remain unchanged, due to the projected area for most LAD projection functions, G(θ), being equivalent at this viewing angle (Nilson, 1971; Wilson, 1963). Woodgate et al. (2015a) demonstrated the coupling effect of view angle and canopy element angle for the tree models used in this study, shown for the 0° and 57.3° viewing angles using three different LADs. For example, if the tree models were given a planophile LAD, then the proportion of leaf material visible at small zenith angles would increase, and subsequently decrease the mean HP-derived α_{est}.

The mean cumulative α_{est} (green line; **Figure 7**) represented the mean α_{est} value if a mask of all angles larger than the specific zenith angle was applied. The mean cumulative α_{est} at 90° matched almost exactly with α_{ref}, thus indicating that the entire FOV was required to produce the most accurate α_{est} value using the classification method from Sea et al. (2011). Also, as expected the mean α_{est} using the entire image FOV matched to within 0.01 of the slope of the linear RMA equation in **Figure 5**. Although there was a spike in mean α_{est} at 80°, the cumulative α_{est} was only marginally affected, rising from 0.33 at 75° to 0.35 at 90°. The implication of the choice of HP view zenith angle range is discussed later in **Section 3.2.3**.

Figure 7: Woody-to-total plant area evaluation

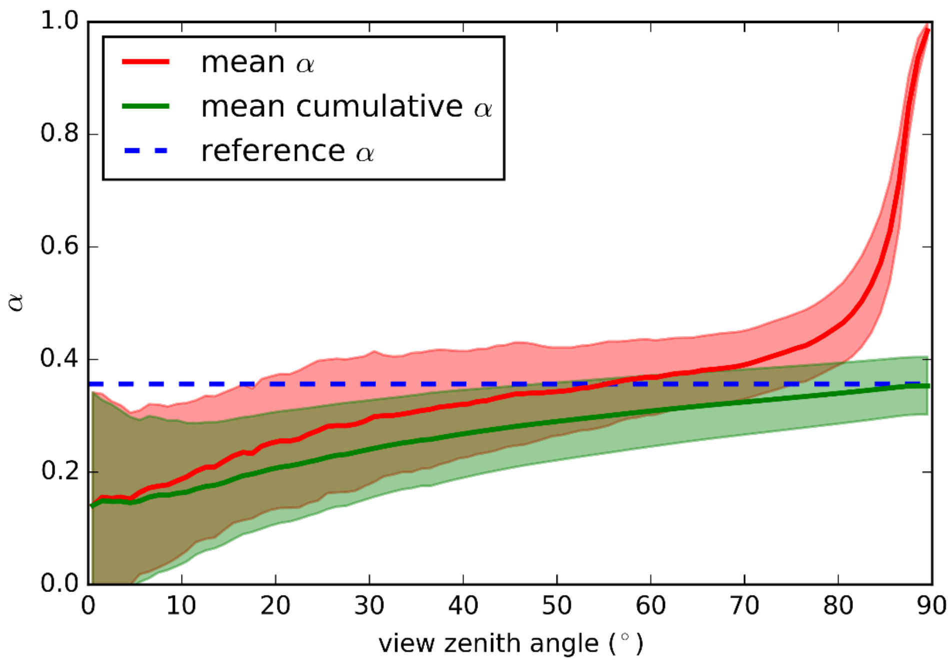

Figure 7. Woody-to-total plant material estimates 'α_{est}' shown as a function of view zenith angle (VZA). α_{est} was estimated as the proportion of woody pixels to total plant pixels from the reference classified HPs. The red line denotes the mean α_{est} value for all 312 simulated HPs at that specific zenith angle; the green line denotes the cumulative mean α_{est} value i.e. the mean α_{est} if a mask of all angles larger than the VZA was applied; the dashed blue line denotes the reference α 'α_{ref}' value > 1.5m (camera height) of all scenes. α_{ref} is independent of zenith angle. The mean α_{est} and mean cumulative α_{est} ±1 standard deviation are denoted by the shaded areas.

Impact of PAI, stem density, and stem distribution on indirect woody-to-total plant area

Further analysis was undertaken to quantify the effect of varying PAI, stem density, and stem distribution on α_{est} from the simulated classified HPs. **Figure 8** shows the mean α_{est} of each simulated scene, estimated from the classified HPs using their entire FOV. This mean estimate is in contrast to the derivation of α using the RMA regression slope of the entire HP population, yet was shown to be approximate equivalent in the previous section. The two scenes with the largest differences in mean α_{est} to α_{ref} were Regular (v:m 1; PAI 0.6) and Random (v:m 0.5; PAI 2.4), with α differences of -0.05 and +0.04, respectively. A distinct PAI effect was observed, with the mean α_{est} slightly increasing with scene PAI. The mean α_{est} of all the scene PAI values were statistically significantly different to one another ($p < 0.05$, Tukey's HSD test), with the exception of PAI scenes = 1.2 & 1.8. This demonstrated that the mean α_{est} using the entire FOV was sensitive to both stem density (PAI = 0.6, 1.2, 1.8) and, to a lesser extent, the size of the trees whilst keeping the stem density constant (e.g. PAI = 2.4).

Figure 8: Scene mean woody-to-total plant area estimates

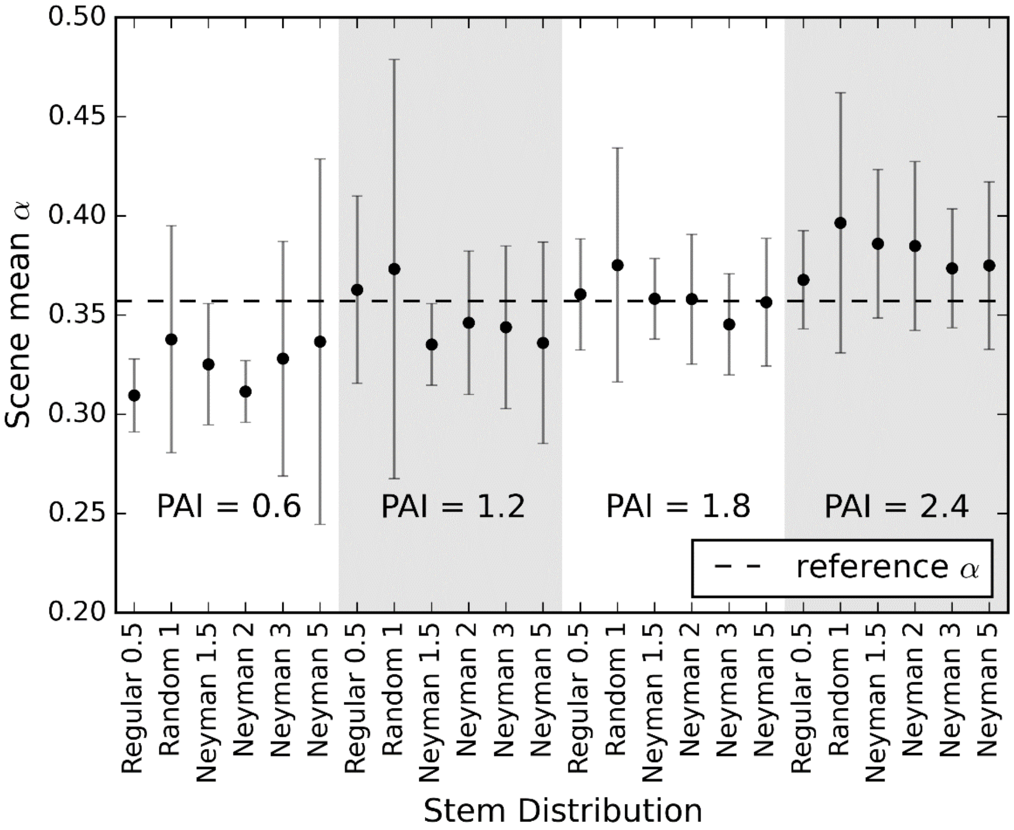

Figure 8. Mean α_{est} of the 24 individual scenes with ±1 standard deviation shown as error bars. The *v:m* for each scene is listed after the stem distribution type on the x-axis. For each PAI scene value, the stem distributions are ordered by *v:m* value (lowest to highest = left to right). Each scenes mean α_{est} was estimated as the ratio of woody pixels to total plant pixels using the entire field-of-view of the simulated classified HPs comprising the scene. The α_{ref} value (dashed line) was calculated as the ratio of the summation of total woody-to-plant facet area for the simulated scenes, and is equivalent for every scene (**Eqn. 3**).

When grouping all scenes into stem distribution, no group was significantly different from any another ($p \geq 0.197$). Therefore, stem distribution did not appear to have any ability to explain differences in mean α_{ref} for each simulated scene. This demonstrates the robustness of the indirect α_{ref} method to varying stem distributions. The three scenes with the largest standard deviations, namely Neyman 5 (PAI 0.6), Random 1 (PAI 1.2), and Random 1 (PAI 2.4), each contained one HP image outlier as shown in **Figure 5 & Figure 6**. These outliers largely explained their comparative higher level of variability. Therefore, the variation in mean α_{ref} for each scene PAI grouping was predominantly a function of sampling position, and not caused by varying stem distribution.

An alternative approach to the empirical method of Sea et al. (2011) is to employ the basic *Pgap* model described by **Eqn. 1** and compute an effective α using the ratio of effective wood and leaf area index. Development of such a model may provide a method more transferable to other canopy types with different structure and result in more physically realistic estimates of α outside the range of woody and plant cover tested in this study. Results are not presented for brevity, however this approach provided a slightly worse fit to the model of Sea et al. (2011) likely due to clumping changing the observed *Pgap* values from that expected from a theoretically independent and random distribution of leaf and wood material. Parameters describing clumping of leaf and wood canopy elements and their degree of mutual occlusion would be required, which are hard to measure separately and efficiently *in-situ* using traditional techniques. Co-registration of TLS point clouds from multiple locations to reduce occlusion effects offers a promising avenue for further research on more direct estimation of α.

The applicability of the method in the field

A potential limitation of the HP classification approach is that optimally-exposed images for accurate *Pgap* estimation usually have poor contrast between wood and leaf canopy elements, due to maximising contrast between sky and non-sky elements (Zhang et al., 2005). The method evaluated here was not subject to any classification errors, due to the material type also being returned for canopy intercepts for the simulated HPs. In the field, if one alters the camera exposure to gain contrast between leaf and woody elements, then the image is likely to be over-exposed, leading to higher *Pgap* than from 'optimally' exposed images. An alternative to HP is to capture multi-angular images using narrow FOV digital cover photography methods (Hwang et al., 2016; Macfarlane et al., 2007b; Macfarlane et al., 2014; Piayda et al., 2015). The comparatively higher image resolution over the same image sampling domain has the advantage of being less sensitive to exposure (Blennow, 1995). For example, Piyada et al. (2015) separated leaf from woody material using an object-based image analysis technique to estimate α using the cover photography method.

The method validated in this study is also applicable to the estimation of LAI using Terrestrial Laser Scanners, which have been used to separate leaf from wood intercepts, e.g. (Danson et al., 2014; Malenovský et al., 2008). TLS uses the intensity information of target structural and spectral properties in the return signal to distinguish between different target types (e.g. Béland et al., 2014). Dual wavelength scanners can account for partial laser beam interceptions and separate leaf and wood purely based on their spectral properties (e.g. Douglas et al., 2015). Additional processing via return classification algorithms using structural knowledge of tree architecture may be used to constrain classification and lead to increased classification accuracy, and thus a better α estimate (e.g. Raumonen et al., 2013).

Each application of this method would require the RMA regression model fit to be established, and for potential outlier images, plots or regions to be identified, especially when characterising large areas. The coefficient of determination provides an indication of the degree of model fit. This step could be first applied to a subset of images, or the entire sample if employing automated classification methods. If outlier plots or regions are found, then separate α estimates may be appropriate for applicable regions. The indirect method tested here is a more attractive alternative than destructive harvesting. Furthermore, the methodology validated in this study could be used to monitor defoliation or regeneration events from numerous ecological causes such as insect attacks, fire, senescence, and phenology.

Potential errors arising from camera exposure and classification accuracy from these *Pgap* and material classification steps are required to be taken into consideration in the field environment, yet were avoided in the modelling and simulation framework. This is an illustration of the modelling and simulation framework more robustly establishing the accuracy of these retrieval methods than in a field environment. It is expected that the performance of the retrieval method investigated in this study will vary depending on forest type, based on the architecture of the trees and relative positioning of crowns. For example, multi-layer forests with vastly different crown shapes and foliage densities are expected to provide differing effective α estimates as a function of view zenith angle to those presented in this study. Dense coniferous species with a low crown break are expected to lead to an underestimation of α following classification (or masking) techniques as a result of a relatively greater proportion of wood occluded by foliage from the typical ground-based measurement perspective. Therefore, it is recommended that a similar 3D simulation framework be applied to different representative reconstructed forest types in order to investigate the robustness of the method validated in this study.

Conclusion

We present validation of a simple and efficient indirect retrieval method to estimate the proportion of woody-to-total plant material 'α' present in a canopy. The method is applicable to all instruments capable of separating leaf from woody elements, such as photography and TLS. A 3D modelling and simulation framework was used to validate the method, parameterised with a representative Eucalypt forest stand comprising highly-detailed 3D explicit reconstructed tree models. The framework enabled the α retrieval method to be validated against precisely known virtual scene parameters consisting of a range of LAI values, stem densities, and stem distributions.

The indirect α method utilising classified HP imagery matched to within on average 0.01 α of the reference values. Quantifying accuracies to this tolerance is near impossible with field-based comparison or benchmarking studies, which are subject to large, hard to quantify, margins of error. In addition, the method was robust to a range of LAI, stem density, and stem distribution values, matching to within ±0.05 α of the true value. This demonstrated its applicability for accurate indirect estimation in the single-storey forest type investigated. Angular dependence on indirect α retrieval was also found; where the entire HP image (180° FOV) was needed to produce the most accurate estimate. Conversely, the classified narrow view zenith angle range around 55-60° zenith also provided α estimates matching the reference. As such, careful consideration of zenith angle ranges utilised from any instrument is recommended.

The method can be used to convert estimates of PAI into LAI. Quantitative α estimates can also be used to aid in the interpretation of the remote sensing signal from satellite data, which have been shown to be sensitive to the proportion and spatial distribution of woody material within the canopy. Suggested future work includes applying the 3D modelling framework to different forest types to determine its accuracy and robustness, e.g. tall or multi-layered forests; including species with different woody proportions, leaf angle distributions, and crown characteristics.

Acknowledgments

The authors would like to acknowledge and thank various sources that provided support for this study. The funding that supported this study came from the Australian Postgraduate Award and Cooperative Research Centre for Spatial Information (CRC-SI). The CRC-SI’s activities are funded in part by the Australian Commonwealth's Cooperative Research Centres Programme. Thanks all who assisted with fieldwork at Rushworth, namely: Tapasya Arya, Andrew Clark, Sam Matthews, Andrew Mellor and Vaibhav Gupta. We would also like to thank Craig Macfarlane for supplying the HP image processing software.

Appendix A: Virtual scene stem placement additional information

For the random and Neyman stem distributions, the placement of the stems was random within each quadrat, consistent with the Neyman Type A distribution (Neyman, 1939). For all virtual scenes, there was a minimum distance of 0.3 m between tree stem centroids to avoid direct overlap of stems. The assignment of a tree model to a stem location was random within the scene, with the exception of the largest trees in the scene, i.e. those with DBH > 40 cm (approximately 5% of trees). These trees were spaced furthest apart in the scenes to ensure they did not unrealistically aggregate.

Scene LAI/PAI values were determined via the number of tree models used and their proportion, and kept constant for each stem distribution. This ensured the within-crown foliage density remained unchanged due to the individual tree models comprising a scene remaining unchanged. For the first three PAI scene values, namely PAI = 0.6, 1.2, and 1.8 corresponding to the stem densities of 186, 372, and 558 trees per 8100 m^2, the same proportions of tree models were used to ensure unchanged proportions of within-crown clumping from individual tree models. The virtual scene tree composition was derived from representative field measurement proportions of species, height, and DBH (*refer to Woodgate et al. (2015a) for more information*).

The same proportion of tree models used for each different scene PAI value also led to a constant factor of 0.6 PAI increase for PAI = 0.6, 1.2, and 1.8 scenes. For the fourth PAI scene value (PAI = 2.4), the same stem distribution maps from PAI = 1.8 scenes were used with an equivalent stem density, where a greater proportion of higher LAI trees were used to gain the higher scene PAI value. The same density was chosen for scenes with PAI = 2.4 as PAI = 1.8, instead of the linear increase in stem density (186 trees per scene PAI value) used in the first three PAI scene values. This was because the 558 stem density was almost equivalent to the maximum value measured in Rushworth plots, yet the PAI of 2.4 was still realistic compared with field measured values (Table 2). Therefore, priority was given to simulations of realistic stem density scenarios guided by field measurements over unrealistic scenarios.

The ALS profile was smooth and normally distributed with greater variance than the simulated scene PAI profiles. This was primarily due to the finite sample size of tree models used in the virtual scenes (n = 51), which were cloned to produce a higher stem density and LAI value within the scene. In other words, there was a greater degree of natural variation between individual trees at the field sites than the reconstructed tree model population comprising the virtual scenes. In addition, the same tree proportions comprising the virtual scenes were used for PAI scene values = 0.6, 1.2, and 1.8. The scenes with a PAI = 2.4 was displayed separately from the first three PAI scene values due to selecting larger trees to increase the scene PAI, while keeping the stem numbers and distributions equal to the scenes with PAI = 1.8. This factor also caused the standard deviations of the simulated scenes height profiles to be comparatively smaller than the ALS profile.

The small variance in the simulated height profiles was due to low variation in occlusion of elements from the different stem distributions for each PAI scene value (**Fig. 4**). This was also a reason why the two 'peaks' start to appear in the simulated data, because the same tree model proportion was used for each scene comprising a specific scene PAI value, rather than varying the tree models selected comprising each scene. Constant tree model proportions for each PAI scene value was deliberate to aid with interpreting stem clumping results. This prevented biasing results from implementing different tree models that may have variable levels of within-crown clumping. It is also noteworthy that 1st returns from *librat* simulated height profiles were derived from an infinitely small beam, whereas ALS had a larger beam diameter (≈20-30 cm diameter at the canopy level). Although the occlusion is the same from both the simulated and ALS captured profiles, the beam divergence may impact on the vertical distribution of the retrieved canopy element profiles.

Table 2. Forest inventory plot details used as input for the virtual scene creation process. RF1-9 relate to the nine forest inventory plots in the 3 km x 3 km study area; R06-08 are the ancillary CCAP inventory plots. The LAI was calculated from the allometric relationships developed from the destructive harvest data (Woodgate et al., 2015a). Trees < 10 cm DBH were not included for stem density or LAI calculations. Stem densities per ha and per 8100 m^{-2} (matching the 90 m x 90 m virtual scene domain) are provided.

Plot name	**Area m^2**	**Stem density ha^{-1} (8100 m^{-2})**	**LAI m^2m^{-2}**
RF1	400	700 (567)	1.10
RF2	400	550 (446)	0.69
RF3	400	550 (446)	1.20
RF4	400	675 (547)	1.68
RF5	400	300 (243)	0.93
RF6	400	575 (466)	0.66
RF7	400	325 (263)	0.58
RF8	400	400 (324)	1.06
RF9	400	625 (507)	1.94
R06	5027	219 (177)	0.69
R07	5027	213 (172)	0.69
R08	5027	563 (456)	1.22

Figure A9: Rushworth Measured Stem clumping

Figure A1. Variance-to-mean ratio '*v:m*' of tree stems calculated at different quadrat sizes for the three 80 m diameter field plots (R06-R08), in addition to the nine forest inventory plots (RF1-9) equivalent to a single quadrat length of 20 m. The joined lines indicate the *v:m* value at a 1 m quadrat length increment below 20 m in length for the R06-R08 field plots. Field plot locations and measurement details are explained in Woodgate et al. (2015a). The 'random' threshold at *v:m* 1 is denoted by the dashed line, with the values above and below the threshold corresponding to increasingly clumped and regular stem distributions, respectively.

References

Armston, J., Disney, M., Lewis, P., Scarth, P., Phinn, S., Lucas, R., Bunting, P., & Goodwin, N. (2013). Direct retrieval of canopy gap probability using airborne waveform lidar. *Remote Sensing of Environment, 134*(0), 24-38. doi: http://dx.doi.org/10.1016/j.rse.2013.02.021

Armston, J.D., Denham, R.J., Danaher, T.J., Scarth, P.F., & Moffiet, T.N. (2009). Prediction and validation of foliage projective cover from Landsat-5 TM and Landsat-7 ETM+ imagery. *Journal of Applied Remote Sensing, 3*, 033540.

Asner, G.P. (1998). Biophysical and Biochemical Sources of Variability in Canopy Reflectance. *Remote Sensing of Environment, 64*(3), 234-253. doi: http://dx.doi.org/10.1016/S0034-4257(98)00014-5

Baret, F., Weiss, M., Allard, D., Garrigues, S., Leroy, M., Jeanjean, H., Fernandes, R., Myneni, R., Privette, J., & Morisette, J. (2005). VALERI: a network of sites and a methodology for the validation of medium spatial resolution land satellite products. *Remote Sensing of Environment*.

Blennow, K. (1995). Sky View Factors from High-Resolution Scanned Fish-eye Lens Photographic Negatives. *Journal of Atmospheric and Oceanic Technology, 12*(6), 1357-1362. doi: 10.1175/1520-0426(1995)012<1357:SVFFHR>2.0.CO;2

Bréda, N.J.J. (2003). Ground-based measurements of leaf area index: A review of methods, instruments and current controversies. *Journal of Experimental Botany, 54*(392), 2403-2417. doi: 10.1093/jxb/erg263

Calders, K., Newnham, G., Burt, A., Murphy, S., Raumonen, P., Herold, M., Culvenor, D., Avitabile, V., Disney, M., Armston, J., & Kaasalainen, M. (2015). Nondestructive estimates of above-ground biomass using terrestrial laser scanning. *Methods in Ecology and Evolution, 6*(2), 198-208. doi: 10.1111/2041-210X.12301

Camacho, F., Cernicharo, J., Lacaze, R., Baret, F., & Weiss, M. (2013). GEOV1: LAI, FAPAR essential climate variables and FCOVER global time series capitalizing over existing products. Part 2: Validation and intercomparison with reference products. *Remote Sensing of Environment, 137*(0), 310-329. doi: http://dx.doi.org/10.1016/j.rse.2013.02.030

Chen, J.M. (1996). Optically-based methods for measuring seasonal variation of leaf area index in boreal conifer stands. *Agricultural and Forest Meteorology, 80*(2-4), 135-163. doi: 10.1016/0168-1923(95)02291-0

Chen, J.M., & Black, T.A. (1992). Defining leaf area index for non-flat leaves. *Plant, Cell & Environment, 15*(4), 421-429.

Chen, J.M., Blanken, P.D., Black, T.A., Guilbeault, M., & Chen, S. (1997a). Radiation regime and canopy architecture in a boreal aspen forest. *Agricultural and Forest Meteorology, 86*(1–2), 107-125. doi: 10.1016/s0168-1923(96)02402-1

Chen, J.M., & Leblanc, S.G. (1997). A four-scale bidirectional reflectance model based on canopy architecture. *IEEE Transactions on Geoscience and Remote Sensing, 35*, 1316-1337. doi: 10.1109/36.628798

Chen, J.M., Rich, P.M., Gower, S.T., Norman, J.M., & Plummer, S. (1997b). Leaf area index of boreal forests: Theory, techniques, and measurements. *J. Geophys. Res., 102*(D24), 29429-29443. doi: 10.1029/97jd01107

Côté, J.-F., Widlowski, J.-L., Fournier, R.A., & Verstraete, M.M. (2009). The structural and radiative consistency of three-dimensional tree reconstructions from terrestrial lidar. *Remote Sensing of Environment, 113*(5), 1067-1081. doi: http://dx.doi.org/10.1016/j.rse.2009.01.017

Danson, F.M., Gaulton, R., Armitage, R.P., Disney, M., Gunawan, O., Lewis, P., Pearson, G., & Ramirez, A.F. (2014). Developing a dual-wavelength full-waveform terrestrial laser scanner to characterize forest canopy structure. *Agricultural and Forest Meteorology, 198–199*(0), 7-14. doi: http://dx.doi.org/10.1016/j.agrformet.2014.07.007

Deblonde, G., Penner, M., & Royer, A. (1994). Measuring Leaf Area Index with the Li-Cor LAI-2000 in Pine Stands. *Ecology, 75*(5), 1507-1511.

Disney, M.I., Lewis, P., Gomez-Dans, J., Roy, D., Wooster, M.J., & Lajas, D. (2011). 3D radiative transfer modelling of fire impacts on a two-layer savanna system. *Remote Sensing of Environment, 115*(8), 1866-1881. doi: http://dx.doi.org/10.1016/j.rse.2011.03.010

Disney, M.I., Lewis, P., & North, P.R.J. (2000). Monte Carlo ray tracing in optical canopy reflectance modelling. *Remote Sensing Reviews, 18*(2-4), 163-196. doi: 10.1080/02757250009532389

Fernandes, R., Plummer, S., Nightingale, J., Baret, F., Camacho, F., Fang, H., Garrigues, S., Gobron, N., Lang, M., Lacaze, R., LeBlanc, S., Meroni, M., Martinez, B., Nilson, T., Pinty, B., Pisek, J., Sonnentag, O., Verger, A., Welles, J., Weiss, M., & Widlowski, J.L. (2014). *Global Leaf Area Index Product Validation Good Practices. Version 2.0* (G. Schaepman-Strub, M. Román & J. Nickeson Eds.): Land Product Validation Subgroup (WGCV/CEOS).

Franklin, J., Michaelsen, J., & Strahler, A.H. (1985). Spatial analysis of density dependent pattern in coniferous forest stands. *Vegetation, 64*(1), 29-36.

Franklin, J.F., & Spies, T.A. (1991). Composition, function, and structure of old-growth Douglas-fir forests. *USDA Forest Service general technical report PNW-GTR-Pacific Northwest Research Station*.

Garrigues, S., Lacaze, R., Baret, F., Morisette, J., Weiss, M., Nickeson, J., Fernandes, R., Plummer, S., Shabanov, N., & Myneni, R. (2008). Validation and intercomparison of global Leaf Area Index products derived from remote sensing data. *Journal of Geophysical Research: Biogeosciences (2005–2012), 113*(G2).

GCOS. (2011). Systematic observation requirements for satellite-based data products for climate. In W. M. Organization (Ed.), (Vol. 154). Switzerland: GCOS.

Gower, S.T., Kucharik, C.J., & Norman, J.M. (1999). Direct and indirect estimation of leaf area index, f(APAR), and net primary production of terrestrial ecosystems. *Remote Sensing of Environment, 70*(1), 29-51. doi: 10.1016/s0034-4257(99)00056-5

Gower, S.T., Vogel, J.G., Norman, J.M., Kucharik, C.J., Steele, S.J., & Stow, T.K. (1997). Carbon distribution and aboveground net primary production in aspen, jack pine, and black spruce stands in Saskatchewan and Manitoba, Canada. *Journal of Geophysical Research: Atmospheres, 102*(D24), 29029-29041. doi: 10.1029/97JD02317

Hagihara, A., & Yamaji, K. (1993). Interception of photosynthetic photon flux density by woody elements in a hinoki (Chamaecyparis obtusa [Sieb. et Zucc.] Endl.) stand. *Ecological Research, 8*(3), 313-318. doi: 10.1007/BF02347190

Hardwick, S.R., Toumi, R., Pfeifer, M., Turner, E.C., Nilus, R., & Ewers, R.M. (2015). The relationship between leaf area index and microclimate in tropical forest and oil palm plantation: Forest disturbance drives changes in microclimate. *Agricultural and Forest Meteorology, 201*(0), 187-195. doi: http://dx.doi.org/10.1016/j.agrformet.2014.11.010

Homolová, L., Malenovský, Z., Hanuš, J., Tomášková, I., Dvořáková, M., & Pokorný, R. (2007). *Comparaison of different ground techniques to map leaf area index of Norway spruce forest canopy*.

Hwang, Y., Ryu, Y., Kimm, H., Jiang, C., Lang, M., Macfarlane, C., & Sonnentag, O. (2016). Correction for light scattering combined with sub-pixel classification improves estimation of gap fraction from digital cover photography. *Agricultural and Forest Meteorology, 222*, 32-44. doi: http://dx.doi.org/10.1016/j.agrformet.2016.03.008

Jacobs, M.R. (1955). Growth Habits of the Eucalypts. Canberra: Forestry and Timber Bureau.

Jennings, S.B., Brown, N.D., & Sheil, D. (1999). Assessing forest canopies and understorey illumination: Canopy closure, canopy cover and other measures. *Forestry, 72*(1), 59-73.

Jonckheere, I., Fleck, S., Nackaerts, K., Muys, B., Coppin, P., Weiss, M., & Baret, F. (2004). Review of methods for in situ leaf area index determination Part I. Theories, sensors and hemispherical photography. *Agricultural and Forest Meteorology, 121*(1-2), 19-35. doi: 10.1016/j.agrformet.2003.08.027

Jonckheere, I., Nackaerts, K., Muys, B., van Aardt, J., & Coppin, P. (2006). A fractal dimension-based modelling approach for studying the effect of leaf distribution on LAI retrieval in forest canopies. *Ecological Modelling, 197*(1–2), 179-195. doi: http://dx.doi.org/10.1016/j.ecolmodel.2006.02.036

Kowalczyk, E., Stevens, L., Law, R., Dix, M., Wang, Y., Harman, I., Haynes, K., Srbinovsky, J., Pak, B., & Ziehn, T. (2013). The land surface model component of ACCESS: description and impact on the simulated surface climatology. *Aust Meteorol Oceanogr J, 63*, 65-82.

Kucharik, C.J., Norman, J.M., & Gower, S.T. (1998). Measurements of branch area and adjusting leaf area index indirect measurements. *Agricultural and Forest Meteorology, 91*(1–2), 69-88. doi: http://dx.doi.org/10.1016/S0168-1923(98)00064-1

Kucharik, C.J., Norman, J.M., Murdock, L.M., & Gower, S.T. (1997). Characterizing canopy nonrandomness with a multiband vegetation imager (MVI). *Journal of Geophysical Research: Atmospheres, 102*(D24), 29455-29473. doi: 10.1029/97JD01175

Leblanc, S. (2008). DHP-TRACWin Manual (Vol. 1.0.3). Centre Spatial John H. Chapman, Québec, Canada: Natural Resources Canada, Canada Centre for Remote Sensing.

Leblanc, S.G., & Chen, J.M. (2001). A practical scheme for correcting multiple scattering effects on optical LAI measurements. *Agricultural and Forest Meteorology, 110*(2), 125-139. doi: 10.1016/s0168-1923(01)00284-2

Leblanc, S.G., Chen, J.M., Fernandes, R., Deering, D.W., & Conley, A. (2005). Methodology comparison for canopy structure parameters extraction from digital hemispherical photography in boreal forests. *Agricultural and Forest Meteorology, 129*(3–4), 187-207. doi: 10.1016/j.agrformet.2004.09.006

Leblanc, S.G., & Fournier, R.A. (2014). Hemispherical photography simulations with an architectural model to assess retrieval of leaf area index. *Agricultural and Forest Meteorology, 194*(0), 64-76. doi: http://dx.doi.org/10.1016/j.agrformet.2014.03.016

Lewis, P. (1999). Three-dimensional plant modelling for remote sensing simulation studies using the Botanical Plant Modelling System. *Agronomie, 19*(3-4), 185-210.

Liu, Z., Jin, G., & Qi, Y. (2012). Estimate of Leaf Area Index in an Old-Growth Mixed Broadleaved-Korean Pine Forest in Northeastern China. *PLoS ONE, 7*(3), e32155. doi: 10.1371/journal.pone.0032155

Lovell, J.L., Jupp, D.L.B., Culvenor, D.S., & Coops, N.C. (2003). Using airborne and ground-based ranging lidar to measure canopy structure in Australian forests. *Canadian Journal of Remote Sensing, 29*(5), 607-622. doi: 10.5589/m03-026

Macfarlane, C. (2011). Classification method of mixed pixels does not affect canopy metrics from digital images of forest overstorey. *Agricultural and Forest Meteorology, 151*(7), 833-840. doi: http://dx.doi.org/10.1016/j.agrformet.2011.01.019

Macfarlane, C., Arndt, S.K., Livesley, S.J., Edgar, A.C., White, D.A., Adams, M.A., & Eamus, D. (2007a). Estimation of leaf area index in eucalypt forest with vertical foliage, using cover and fullframe fisheye photography. *Forest Ecology and Management, 242*(2–3), 756-763. doi: 10.1016/j.foreco.2007.02.021

Macfarlane, C., Grigg, A., & Evangelista, C. (2007b). Estimating forest leaf area using cover and fullframe fisheye photography: Thinking inside the circle. *Agricultural and Forest Meteorology, 146*(1–2), 1-12. doi: 10.1016/j.agrformet.2007.05.001

Macfarlane, C., Ryu, Y., Ogden, G.N., & Sonnentag, O. (2014). Digital canopy photography: Exposed and in the raw. *Agricultural and Forest Meteorology, 197*(0), 244-253. doi: http://dx.doi.org/10.1016/j.agrformet.2014.05.014

Malenovský, Z., Martin, E., Homolová, L., Gastellu-Etchegorry, J.-P., Zurita-Milla, R., Schaepman, M.E., Pokorný, R., Clevers, J.G.P.W., & Cudlín, P. (2008). Influence of woody elements of a Norway spruce canopy on nadir reflectance simulated by the

DART model at very high spatial resolution. *Remote Sensing of Environment, 112*(1), 1-18. doi: 10.1016/j.rse.2006.02.028

Neumann, H.H., Den Hartog, G., & Shaw, R.H. (1989). Leaf area measurements based on hemispheric photographs and leaf-litter collection in a deciduous forest during autumn leaf-fall. *Agricultural and Forest Meteorology, 45*(3-4), 325-345.

Neyman, J. (1939). On a New Class of "Contagious" Distributions, Applicable in Entomology and Bacteriology. *The Annals of Mathematical Statistics, 10*(1), 35-57. doi: 10.2307/2235986

Nilson, T. (1971). A theoretical analysis of the frequency of gaps in plant stands. *Agricultural Meteorology, 8*(C), 25-38.

Piayda, A., Dubbert, M., Werner, C., Vaz Correia, A., Pereira, J.S., & Cuntz, M. (2015). Influence of woody tissue and leaf clumping on vertically resolved leaf area index and angular gap probability estimates. *Forest Ecology and Management, 340*(0), 103-113. doi: http://dx.doi.org/10.1016/j.foreco.2014.12.026

Raumonen, P., Kaasalainen, M., Åkerblom, M., Kaasalainen, S., Kaartinen, H., Vastaranta, M., Holopainen, M., Disney, M., & Lewis, P. (2013). Fast automatic precision tree models from terrestrial laser scanner data. *Remote Sensing, 5*(2), 491-520.

Ross, J. (1981). *The radiation regime and architecture of plant stands*. London: Junk.

Schaefer, M.T., Farmer, E., Soto-Berelov, M., Woodgate, W., & Jones, S. (2015). Overview of ground based techniques for estimating LAI. In M. Soto-Berelov, A. Held, S. Phinn & S. Jones (Eds.), *AusCover Good Practice Guidelines: A technical handbook supporting calibration and validation activities of remotely sensed data products* (pp. 88-118). http://data.auscover.org.au/xwiki/bin/view/Good+Practice+Handbook/WebHome: TERN AusCover.

Sea, W.B., Choler, P., Beringer, J., Weinmann, R.A., Hutley, L.B., & Leuning, R. (2011). Documenting improvement in leaf area index estimates from MODIS using hemispherical photos for Australian savannas. *Agricultural and Forest Meteorology, 151*, 1453–1461. doi: 10.1016/j.agrformet.2010.12.006

Tang, H., Brolly, M., Zhao, F., Strahler, A.H., Schaaf, C.L., Ganguly, S., Zhang, G., & Dubayah, R. (2014). Deriving and validating Leaf Area Index (LAI) at multiple spatial scales through lidar remote sensing: A case study in Sierra National Forest, CA. *Remote Sensing of Environment, 143*(0), 131-141. doi: http://dx.doi.org/10.1016/j.rse.2013.12.007

Verrelst, J., Schaepman, M.E., Malenovský, Z., & Clevers, J.G.P.W. (2010). Effects of woody elements on simulated canopy reflectance: Implications for forest chlorophyll content retrieval. *Remote Sensing of Environment, 114*(3), 647-656. doi: http://dx.doi.org/10.1016/j.rse.2009.11.004

Walter, J.M.N., Fournier, R.A., Soudani, K., & Meyer, E. (2003). Integrating clumping effects in forest canopy structure: an assessment through hemispherical photographs. *Canadian Journal of Remote Sensing, 29*(3), 388-410.

Whittaker, R.H., & Woodwell, G.M. (1969). Structure, Production and Diversity of the Oak-Pine Forest at Brookhaven, New York. *Journal of Ecology, 57*(1), 155-174. doi: 10.2307/2258214

Widlowski, J.L., Pinty, B., Lopatka, M., Atzberger, C., Buzica, D., Chelle, M., Disney, M., Gastellu-Etchegorry, J.P., Gerboles, M., Gobron, N., Grau, E., Huang, H., Kallel, A., Kobayashi, H., Lewis, P.E., Qin, W., Schlerf, M., Stuckens, J., & Xie, D. (2013). The fourth radiation transfer model intercomparison (RAMI-IV): Proficiency testing of canopy reflectance models with ISO-13528. *Journal of Geophysical Research: Atmospheres, 118*(13), 6869-6890. doi: 10.1002/jgrd.50497

Wilkes, P., Jones, S.D., Suarez, L., Haywood, A., Woodgate, W., Soto-Berelov, M., Mellor, A., & Skidmore, A.K. (2015). Understanding the Effects of ALS Pulse Density for Metric Retrieval across Diverse Forest Types. *Photogrammetric Engineering & Remote Sensing, 81*(8), 625-635. doi: 10.14358/PERS.81.8.625

Wilson, J. (1963). Estimation of foliage denseness and foliage angle by inclined point quadrats. *Australian Journal of Botany, 11*(1), 95-105. doi: http://dx.doi.org/10.1071/BT9630095

Woodgate, W., Disney, M., Armston, J.D., Jones, S.D., Suarez, L., Hill, M.J., Wilkes, P., Soto-Berelov, M., Haywood, A., & Mellor, A. (2015a). An improved theoretical model of canopy gap probability for Leaf Area Index estimation in woody ecosystems. *Forest Ecology and Management, 358*, 303-320. doi: http://dx.doi.org/10.1016/j.foreco.2015.09.030

Woodgate, W., Jones, S.D., Suarez, L., Hill, M.J., Armston, J.D., Wilkes, P., Soto-Berelov, M., Haywood, A., & Mellor, A. (2015b). Understanding the variability in ground-based methods for retrieving canopy openness, gap fraction, and leaf area index in diverse forest systems. *Agricultural and Forest Meteorology, 205*(0), 83-95. doi: http://dx.doi.org/10.1016/j.agrformet.2015.02.012

Zhang, Y., Chen, J.M., & Miller, J.R. (2005). Determining digital hemispherical photograph exposure for leaf area index estimation. *Agricultural and Forest Meteorology, 133*(1–4), 166-181. doi: 10.1016/j.agrformet.2005.09.009

Zheng, G., & Moskal, L.M. (2009). Retrieving Leaf Area Index (LAI) Using Remote Sensing: Theories, Methods and Sensors. *Sensors, 9*(4), 2719-2745.